

Catalysis Science & Technology

Accepted Manuscript



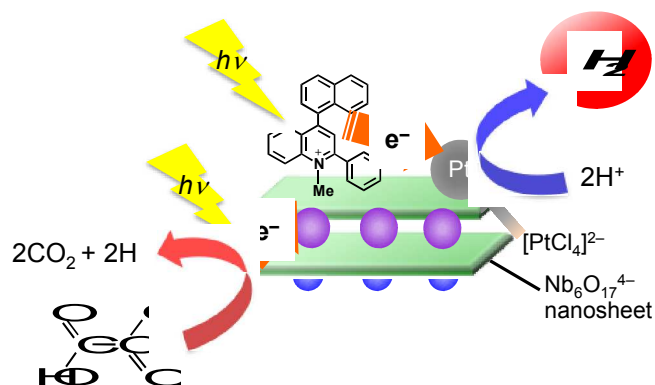
This is an *Accepted Manuscript*, which has been through the Royal Society of Chemistry peer review process and has been accepted for publication.

Accepted Manuscripts are published online shortly after acceptance, before technical editing, formatting and proof reading. Using this free service, authors can make their results available to the community, in citable form, before we publish the edited article. We will replace this *Accepted Manuscript* with the edited and formatted *Advance Article* as soon as it is available.

You can find more information about *Accepted Manuscripts* in the [Information for Authors](#).

Please note that technical editing may introduce minor changes to the text and/or graphics, which may alter content. The journal's standard [Terms & Conditions](#) and the [Ethical guidelines](#) still apply. In no event shall the Royal Society of Chemistry be held responsible for any errors or omissions in this *Accepted Manuscript* or any consequences arising from the use of any information it contains.

Table of Contents



A Pt catalyst was closely located to an organic photosensitizer on a negatively charged semiconductor for efficient photocatalytic H₂ evolution.

Cite this: DOI:
10.1039/x0xx00000x

Received 00th August 2014,
Accepted 00th xxxx 2014

DOI: 10.1039/x0xx00000x

www.rsc.org/

A composite photocatalyst of an organic electron donor-acceptor dyad and a Pt catalyst supported on semiconductor nanosheets for efficient hydrogen evolution from oxalic acid

Yusuke Yamada, Akifumi Nomura, Hideyuki Tadokoro and Shunichi Fukuzumi*

A composite photocatalytic system for hydrogen evolution employing acidic oxalic acid as an electron donor has been successfully constructed by combining 2-phenyl-4-(1-naphthyl)quinolinium ion (QuPh⁺-NA), platinum (Pt) and nanosheets prepared by exfoliation of K₄Nb₆O₁₇ (niobate-NS) as an organic photosensitizer, a hydrogen-evolution catalyst and a semiconductor photocatalyst for oxidation of oxalic acid, respectively. The composite photocatalyst, QuPh⁺-NA/niobate-NS (Pt), was prepared by a two-step route to locate a Pt catalyst near QuPh⁺-NA on the surfaces of niobate-NS: (i) supporting QuPh⁺-NA on niobate-NS by a cation exchange method and then (ii) supporting Pt on the QuPh⁺-NA/niobate-NS by a photodeposition method using PtCl₄²⁻ as a precursor, which repulsively interacts with the negatively charged surfaces of niobate-NS. The precursor of PtCl₄²⁻ was reduced to metallic Pt by the photocatalysis of QuPh⁺-NA in the presence of oxalate. Photocatalytic hydrogen evolution with the composite catalyst proceeds via photoexcitation of both niobate-NS and QuPh⁺-NA to produce an electron and a hole in the semiconductor and the ET state (QuPh⁺-NA^{•+}), respectively. The photogenerated hole of niobate-NS oxidises oxalic acid to produce CO₂ and CO₂^{•-} with two protons, whereas the photogenerated electron and CO₂^{•-} reduce QuPh⁺-NA and the electron-transfer (ET) state to produce two equivalents of QuPh⁺-NA, which inject electrons to the Pt catalyst to reduce protons to hydrogen. Utilization of oxalic acid as an electron donor even under highly acidic conditions, which is thermodynamically favourable for proton reduction to evolve hydrogen but unfavourable for oxalate oxidation, has been made possible for the first time by combining QuPh⁺-NA, Pt and niobate-NS. Composite photocatalysts were also prepared by employing mesoporous silica-alumina and nanosheets prepared by exfoliation of KTiNbO₅ (titanoniobate-NS), which possesses a band structure different from niobate-NS, as supports to clarify the requirements for a building block to achieve an active composite photocatalyst.

Introduction

Hydrogen (H₂) has been regarded as a potential fuel of the next generation because of high energy density per weight and no emission of harmful gases after use.¹ At present, H₂ supplied to industries is mainly produced by the steam reforming reaction of hydrocarbons, mostly natural gas, indicating that H₂ is not a really clean and recyclable fuel.² To be a really clean and recyclable fuel, H₂ should be produced from recyclable resources by utilizing natural energy, such as solar energy.³⁻⁸ In this context, photocatalytic water splitting to produce H₂ and O₂ from water by UV light irradiation has been extensively studied by using metal-oxide semiconductors such as TiO₂ supporting Pt, Ru or Ni.⁹⁻²⁴ The band gaps of semiconductors have been

tuned by doping of nitrogen or sulfur to metal-oxide semiconductors to improve the photoresponse of the semiconductors to visible light for water splitting.²⁵⁻²⁶

In natural photosynthesis, two photosystems (I and II) are combined to achieve both oxidation of water and reduction of nicotinamide adenine dinucleotide (NAD⁺) via the so called Z-scheme for enabling to utilize whole visible light.²⁷ Such a Z-scheme system has been utilized to improve photocatalysis of metal-oxide semiconductors by combining two narrow band-gap semiconductors, which are active for water oxidation and reduction under visible light irradiation, with an electron mediator, enabling to utilize visible light for water splitting.²⁸⁻³² Supporting various types of photosensitisers on semiconductors

has also been widely examined to utilize visible light for water splitting.³³⁻⁴⁰

As compared to semiconductors, energy gaps are much easier to be finely tuned for organic electron donor-acceptor linked molecules which can mimic photoinduced charge separation in the photosynthetic reaction center.⁴¹⁻⁴⁴ Such photosynthetic reaction center models with long lifetimes of charge-separated states have been utilized as photocatalysts together with water reduction catalysts for H₂ evolution, which requires relatively strong electron donors such as NADH because of the absence of efficient oxidation catalysts.⁴⁵⁻⁴⁹ In general, semiconductors are known to act as efficient oxidation catalysts.⁹⁻²⁴ Thus, combination of photosynthetic reaction center models and semiconductors with water reduction catalysts would enable the development of efficient photocatalytic systems for H₂ evolution that is not possible by either of catalytic systems alone. However, such composites of photosynthetic reaction center models for charge separation and inorganic semiconductors have yet to be reported.

We report herein a photocatalytic H₂-evolution system using a composite photocatalyst of an organic electron donor-acceptor linked dyad, 2-phenyl-4-(1-naphthyl)quinolinium ion (QuPh⁺-NA) which has a long lifetime of the electron-transfer (ET) state upon photoexcitation, and a Pt catalyst supported on semiconductor nanosheets derived from K₄Nb₆O₁₇ (niobate-NS) in the presence of acidic oxalic acid as an electron donor. K₄Nb₆O₁₇ supporting Pt or Ni has been reported to act as a photocatalyst for water splitting by using a high pressure mercury lamp.^{23,24} However, niobate-NS, which possesses high surface area suitable for supporting cationic species, exhibits no such activity.³⁷ Oxalic acid is a naturally abundant organic compound, which has been hardly used as an electron donor for photocatalytic hydrogen evolution.⁴⁸⁻⁵¹ The composite catalyst has enabled to use oxalic acid as an electron donor for photocatalytic H₂ evolution by the Z-scheme system (vide supra) in which oxalic acid is oxidised by the hole of semiconductor nanosheets produced upon photoexcitation, whereas water is reduced by photocatalysis of QuPh⁺-NA with a Pt catalyst. The Pt catalyst was deposited in the close vicinity of QuPh⁺-NA by *in situ* reduction of anionic PtCl₄²⁻, which repulsively interacts with anionic surfaces of the semiconductor nanosheets. The close location of the QuPh⁺-NA and the Pt catalyst promotes forward electron transfer from photoexcited QuPh⁺-NA to the Pt catalyst. Additionally, niobate-NS of the composite catalyst was replaced with titanoniobate nanosheets prepared by exfoliation of KTiNbO₅ (titanoniobate-NS) or mesoporous silica-alumina (sAIMCM-41). sAIMCM-41 is photocatalytically inactive but a cation exchangeable material. K₄Nb₆O₁₇ and KTiNbO₅ are semiconductors, which possess cation exchangeable surfaces and strong oxidizing ability by UVA light irradiation.²²⁻²⁴ Comparison of the composite catalysts in terms of photocatalysis for H₂ evolution and oxalic acid oxidation, and the lifetime of photogenerated QuPh⁺-NA^{•+} on each support clarified requirements to achieve an active composite catalyst for the photocatalytic H₂ evolution. Although the present composite photocatalytic system is still

incapable of using water as a reductant for H₂ evolution because of the absence of water oxidation catalyst, combination of an organic photosynthetic reaction center model compound with semiconductor nanosheets and a water reduction catalyst reported for the first time in this study provides a promising perspective for further development of efficient water splitting photocatalytic systems, which may not be achieved by inorganic semiconductors alone without organic charge-separation components.

2. Result and discussion

2.1 Adsorption of QuPh⁺-NA on metal-oxide nanosheets

Metal-oxide semiconductor nanosheets used as the oxidation catalyst of the composite catalyst were prepared by exfoliation of K₄Nb₆O₁₇ and KTiNbO₅ (niobate-NS and titanoniobate-NS) as reported in literature,⁵²⁻⁵⁴ and characterized by powder X-ray diffraction, N₂ adsorption-desorption isotherm and thermogravimetry/differential thermal analysis (TG/DTA) as shown in Figs. S1-S4 in ESI. The morphologies of niobate-NS and titanoniobate-NS were confirmed by TEM observations. Figs. 1a and 1b display TEM images of as-prepared K₄Nb₆O₁₇ and niobate-NS, respectively. The size of as-prepared K₄Nb₆O₁₇ was more than 1 μm and no mesopore was observed. On the other hand, major portions of niobate-NS formed nanoscrolls as observed in previous reports.³⁹ The size of nanoscrolls was about 500-1000 nm × 10-20 nm in the length and diameter as shown in Fig. 1b. Similar scroll morphology was observed for titanoniobate-NS as shown in Fig. 1c although some particles have a sheet morphology as shown in Fig. 1d.

An organic electron donor-acceptor linked dyad of 2-phenyl-4-(1-naphthyl)quinolinium ion (QuPh⁺-NA) was supported on niobate-NS by a cation-exchange method in a mixed solution of MeCN and water [1:1 (v/v)] at room temperature for 4 h. When as-prepared K₄Nb₆O₁₇ was used as a support instead of niobate-NS, only little amount of QuPh⁺-NA was adsorbed because of small Brunauer-Emmett-Teller (BET)

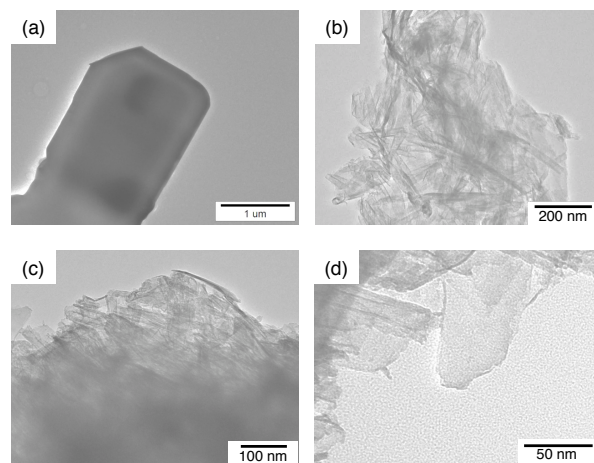


Fig. 1 TEM images of (a) as-prepared K₄Nb₆O₁₇, (b) exfoliated K₄Nb₆O₁₇ (niobate-NS) and (c,d) exfoliated KTiNbO₅ with scroll and sheet morphologies (titanoniobate-NS).

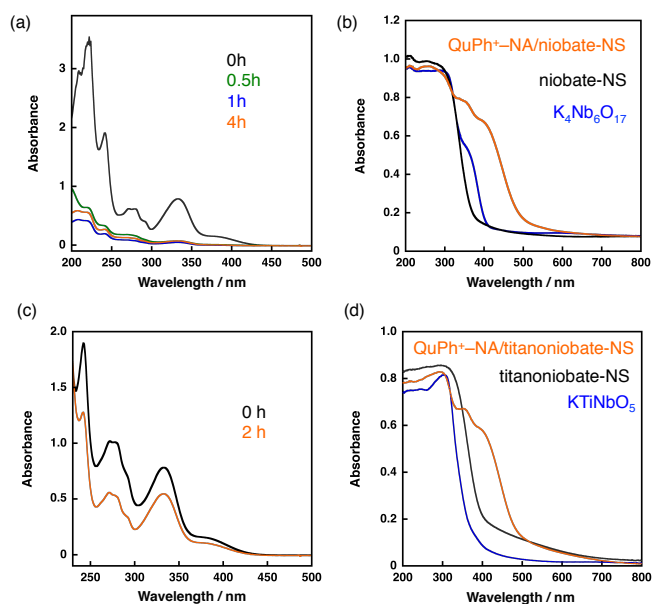


Fig. 2 (a, c) UV-vis absorption change of supernatant containing QuPh⁺-NA by immersion of (a) niobate-NS and (c) titanoniobate-NS. (b, d) Diffused reflectance UV-vis absorption spectra of (b) niobate-NS (black) and QuPh⁺-NA/niobate-NS (orange) and (d) titanoniobate-NS (black) and QuPh⁺-NA/niobate-NS (orange). BaSO₄ was used for background measurements.

surface area ($< 5 \text{ m}^2 \text{ g}^{-1}$). The loading amount of QuPh⁺-NA on niobate-NS was determined to be $1.4 \times 10^{-4} \text{ mol g}^{-1}$ (4.9 wt%) by the UV-vis absorbance change of the supernatant at 334 nm characteristic to QuPh⁺-NA in Fig. 2a.^{49,50} No significant difference was observed between niobate-NS and QuPh⁺-NA/niobate-NS in terms of N₂ adsorption-desorption isotherm and powder X-ray diffraction (Fig. S6 in ESI). The amount of supported QuPh⁺-NA estimated from the weight loss observed in TG analysis was $1.4 \times 10^{-4} \text{ mol g}^{-1}$ (Fig. S7a in ESI), which agrees with the value estimated from the UV-vis spectral change. The adsorbed QuPh⁺-NA on the surface of niobate-NS was detected by diffuse reflectance UV-vis spectroscopy (DRS) by increasing absorption around 400 nm as shown in Fig. 2b. Similarly, the amount of QuPh⁺-NA supported on titanoniobate-NS by the same method was determined to be $5.1 \times 10^{-5} \text{ mol g}^{-1}$ (1.8 wt%, Fig. S7b in ESI). The adsorption of QuPh⁺-NA was confirmed by DRS, in which strong absorption bands appeared at the wavelength longer than 400 nm, (Fig. 2d) and IR absorption spectroscopy (Fig. S8 in ESI).

2.2 Preparation of photocatalysts composed of QuPh⁺-NA/niobate-NS with negatively and positively charged Pt precursors and photocatalysis for H₂ evolution

A composite photocatalyst of QuPh⁺-NA/niobate-NS supporting a Pt catalyst for H₂ evolution [QuPh⁺-NA/niobate-NS (Pt)] was prepared *in situ* by photoirradiation of an aqueous suspension containing QuPh⁺-NA/niobate-NS and K₂PtCl₄ in the presence of oxalic acid. The concentration of K₂PtCl₄ (10 μM) was much smaller than QuPh⁺-NA (0.22 mM) based on the optimization of the concentration of K₂PtCl₄ in the solution (Fig. 5, *vide infra*). Under photoirradiation, photogenerated

electron-transfer (ET) state of QuPh⁺-NA (QuPh⁺-NA^{•+}) reduces K₂PtCl₄ to deposit the metallic Pt catalyst on the surfaces of niobate-NS. The negatively charged [PtCl₄]²⁻ was selected as a precursor to prevent the deposition of Pt²⁺ cations on niobate-NS by the cation exchange. A certain amount of H₂ evolution was observed for the suspension containing QuPh⁺-NA/niobate-NS and K₂PtCl₄ under photoirradiation (Fig. 3a, red circle). The turnover number of Pt for H₂ evolution was 250 with the turnover frequency of 21 h⁻¹ for 12 h. On the other hand, no significant amount of H₂ evolution was observed when niobate-NS without QuPh⁺-NA was used instead of QuPh⁺-NA/niobate-NS (Fig. 3a, black square). Thus, QuPh⁺-NA is necessary for the photocatalytic H₂ evolution. Similarly, no H₂ evolution was observed by employing cationic [Pt(NH₃)₄]²⁺ (Fig. 3a, blue triangle), which is often used to prepare platinized K₄Nb₆O₁₇,^{24,34} as a precursor instead of K₂PtCl₄. In this case, [Pt(NH₃)₄]²⁺ was adsorbed on the cation exchange sites of niobate-NS, to which QuPh⁺-NA is not closely located.

For QuPh⁺-NA/niobate-NS (Pt), CO₂ evolution accompanied with H₂ evolution in nearly two times volume of H₂ was observed (Fig. 3b, red circle), indicating that oxalic acid acted as the electron donor. The ratio of CO₂/H₂ ranging from 1.5 to 2.0 slightly smaller than stoichiometric value (2.0) may result from a small portion of CO₂ dissolved in water. The catalysis of the composite depending on Pt precursors indicates that not only preparation procedures but also choices of precursors are important to obtain an active composite photocatalyst for H₂ evolution.

The scroll morphology of niobate-NS was maintained after formation of QuPh⁺-NA/niobate-NS (Pt) as confirmed by TEM observations (Fig. 4a). The sizes of Pt nanoparticles were too small to be detected by TEM for QuPh⁺-NA/niobate-NS (Pt) after the reaction for 6 h. However, the TEM images of QuPh⁺-NA/niobate-NS (Pt) after the reaction for 19 h show formation of Pt particles smaller than 5 nm (Figs. 4b and 4c). Such grown Pt particles were also observed for the QuPh⁺-NA/niobate-NS [Pt(NH₃)₄]²⁺ after the photoirradiation (Fig. S9 in ESI). The highly dispersed small Pt nanoparticles exhibited the high

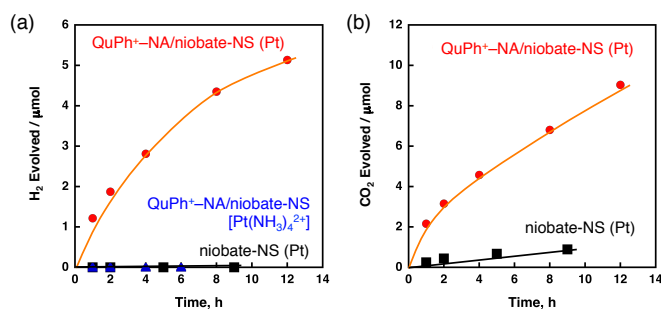


Fig. 3 Time courses of (a) H₂ and (b) CO₂ evolution by photoirradiation ($\lambda > 340 \text{ nm}$) of N₂-saturated aqueous suspensions (2.0 mL, pH 1.6) containing oxalic acid (50 mM), K₂PtCl₄ (10 μM) and niobate-NS (10.0 mg) (black square); oxalic acid (50 mM), K₂PtCl₄ (10 μM) and QuPh⁺-NA/niobate-NS (10.5 mg) (red circle) and oxalic acid (50 mM), Pt(NH₃)₄Cl₂ (10 μM) and QuPh⁺-NA/niobate-NS (10.5 mg) (blue triangle).

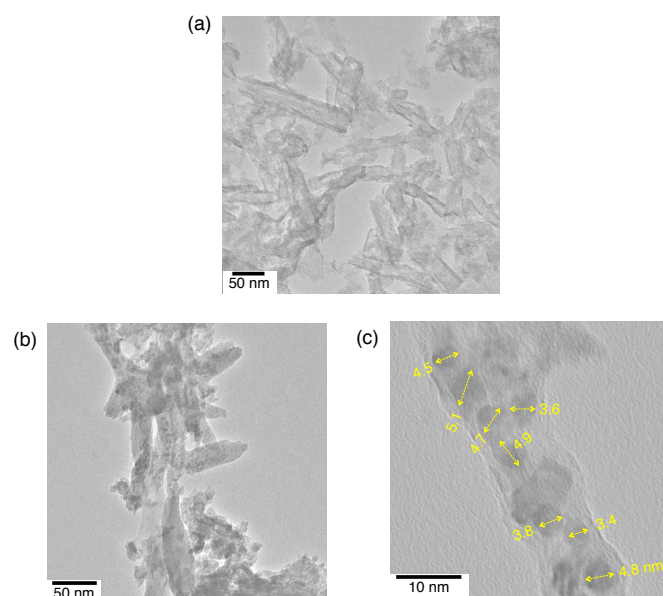


Fig. 4 TEM images of QuPh⁺-NA/niobate-NS (Pt) after the photocatalytic reactions for (a) 6 h and (b, c) 19 h. The numbers indicate the sizes of each Pt nanoparticles in nm.

catalytic activity for H₂ evolution. The DRS of the reaction suspension indicates that nearly half of QuPh⁺-NA supported on niobate-NS lost its colour during the reaction for 12 h (Fig. S5). Thus, the catalytic reactivity was lost as QuPh⁺-NA was reduced and the size of Pt nanoparticles increased.

2.3 Optimization of reaction conditions for photocatalytic H₂ evolution using QuPh⁺-NA/niobate-NS (Pt)

The effect of K₂PtCl₄ concentration on H₂ evolution was investigated for the reaction solution containing K₂PtCl₄, QuPh⁺-NA/niobate-NS and oxalic acid. Fig. 5a shows the time courses of H₂ evolution by photoirradiation of an aqueous suspension containing oxalic acid (50 mM), QuPh⁺-NA/niobate-NS (10.5 mg) and K₂PtCl₄ with various concentrations (2.5–40 μM) at pH 1.6. The initial H₂ evolution rate (1 h) of 0.42 μmol h⁻¹ for the composite photocatalyst prepared in the presence of 2.5 μM K₂PtCl₄ was increased to 1.2 μmol h⁻¹ by increasing the K₂PtCl₄ concentration to 10 μM. If all K₂PtCl₄ are reduced to metallic Pt and deposited on QuPh⁺-NA/niobate-NS, the weight concentration of Pt is 0.37 wt% in the composite photocatalyst derived from 10 μM K₂PtCl₄. When the K₂PtCl₄ concentration was further increased to 20–40 μM, however, the amount of H₂ evolution was significantly decreased (0.49 μmol with 20 μM and 0.14 μmol with 40 μM). Such a decrease in the amount of H₂ evolution may result from the increase in the size of Pt catalyst with the larger concentration of K₂PtCl₄ (20–40 μM) during the photocatalytic reaction. Thus, the optimum K₂PtCl₄ concentration may be about 10 μM.

Then, the effect of the pH of reaction solutions on the H₂ evolution was investigated, because the form of oxalic acid in solution changes from the acid to the monoanion and the

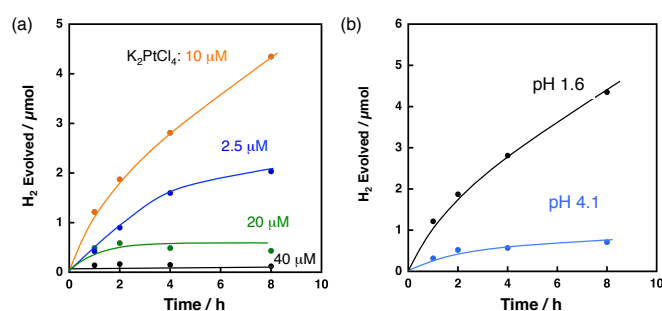


Fig. 5 (a) Time courses of H₂ evolution by photoirradiation ($\lambda > 340$ nm) of an N₂-saturated aqueous suspension (2.0 mL) containing oxalic acid (50 mM), QuPh⁺-NA/niobate-NS (10.5 mg) and various concentrations of K₂PtCl₄ (2.5–40 μM) at pH 1.6. (b) Time courses of H₂ evolution under pH 1.6 and 4.1 conditions. The concentrations of oxalic acid, QuPh⁺-NA/niobate-NS and K₂PtCl₄ were 50 mM, 10.5 mg and 10 μM, respectively. The pH value of each aqueous medium was controlled to 1.6 (black) or 4.1 (cyan) by adding KOH.

dianion depending on the pH of reaction solution. The pK_{a1} and pK_{a2} values of oxalic acid (1.3 and 4.2, respectively)⁵⁵ suggest that oxalate dianion becomes major species in the solution of pH > 4.2. On the other hand, higher pH is thermodynamically unfavourable for proton reduction. Thus, if the oxidation of oxalic acid is a rate-determining step, the reaction rate would become maximum around pH 4.2. If the proton reduction is the rate-determining step, the reaction would become faster at much lower pH. Fig. 5b compares the time courses of H₂ evolution from the reaction solutions containing 10 μM K₂PtCl₄ at pH 1.6 and 4.1 in the photocatalytic H₂ evolution. The initial H₂ evolution rate (1 h) was decreased from 1.2 μmol h⁻¹ at pH 1.6 to 0.32 μmol h⁻¹ at pH 4.1. Therefore, the proton reduction rather than the oxalate oxidation is the rate-determining step for the H₂ evolution in this photocatalytic system.

The effect of irradiance was also examined by using a solar simulator (AM 1.5G). The light source contains both UVA (350 nm < λ < 400 nm) and visible light ($\lambda > 400$ nm). The photocatalytic H₂ evolution was performed by photoirradiation of an aqueous suspension (2.0 mL) in a square quartz cuvette (light path length: 10 mm) containing QuPh⁺-NA/niobate-NS (10.5 mg), K₂PtCl₄ (10 μM) and oxalic acid (10 mM) with changing the irradiance from 0.1 kW m⁻² (0.1 sun) to 1 kW m⁻² (1 sun). The H₂ evolution in the photocatalytic reaction was accelerated by increasing the irradiance up to 0.5 kW m⁻² (0.5 sun), however, further increase of the irradiance resulted in no further increase in the H₂ evolution rate (Fig. S10 in ESI).

2.4 Composite photocatalysts using sAIMCM-41 and titanoniobate-NS as supports

The activity of composite photocatalysts for the photocatalytic H₂ evolution is expected to depend on the supporting materials. Silica-alumina (sAIMCM-41) is a cation exchangeable but insulating material. First, the photocatalytic H₂ evolution was performed under photoirradiation of a highly acidic aqueous suspension (2.0 mL, pH 0.9) containing oxalic acid (50 mM), K₂PtCl₄ (10 μM) and QuPh⁺-NA/sAIMCM-41 (11.6 mg, [QuPh⁺-NA]: 0.22 mM). As indicated in Fig. 6 (black square), no H₂ evolution was observed for QuPh⁺-NA/sAI-MCM-41

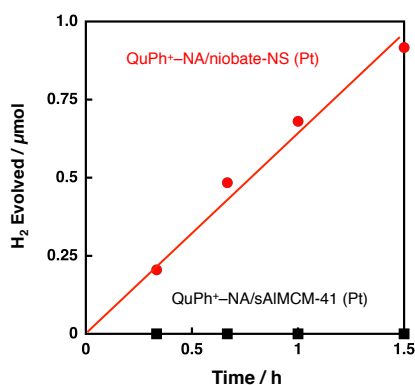


Fig. 6 Time courses of H₂ evolution by photoirradiation ($\lambda > 340$ nm) of an N₂-saturated aqueous H₂SO₄ suspension (100 mM, pH 0.9, 2.0 mL) containing oxalic acid (50 mM), K₂PtCl₄ (10 μ M) and QuPh⁺-NA supported on metal oxides [QuPh⁺-NA/niobate-NS (10.5 mg, red circle); QuPh⁺-NA/sAIMCM-41 (11.6 mg, black square)].

(Pt). Thus, the use of photocatalytically active niobate-NS has made it possible to evolve H₂ under the conditions by utilizing the oxidizing ability, which is strong enough to oxidise acidic oxalic acid.

Then, the activity of a composite photocatalyst using titanoniobate-NS instead of niobate-NS was examined as shown in Fig. 7, where no H₂ evolution was observed under photoirradiation for 5 h (blue square) in contrast with the case of niobate-NS (red circle). The reason of the drastic difference in the photocatalytic activity between titanoniobate-NS and niobate-NS was investigated in the following sections.

2.5 Photocatalytic oxidation of oxalic acid with metal-oxide nanosheets

First, photocatalysis of niobate-NS and titanoniobate-NS for oxalic acid oxidation was confirmed by CO₂ evolution from an O₂-saturated aqueous solution (pH 1.6) containing oxalic acid under photoirradiation ($\lambda > 340$ nm). Fig. 8 shows the time courses of CO₂ evolution under photoirradiation ($\lambda > 340$ nm) of an O₂-saturated aqueous suspension containing oxalic acid and K₄Nb₆O₁₇ or KTiNbO₅. The amount of evolved CO₂ was

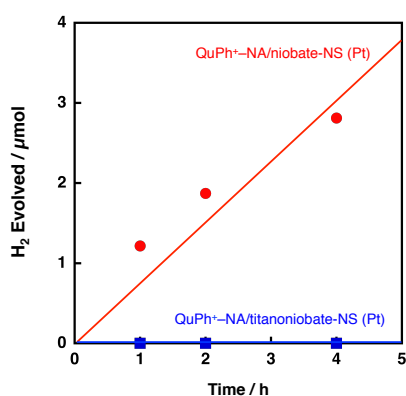


Fig. 7 Time courses of H₂ evolution by photoirradiation ($\lambda > 340$ nm) of an N₂-saturated aqueous suspension (2.0 mL, pH 1.6) containing oxalic acid (50 mM), K₂PtCl₄ (10 μ M) and QuPh⁺-NA/niobate-NS (10.5 mg, red circle) or QuPh⁺-NA/titanoniobate-NS (10.2 mg, blue square).

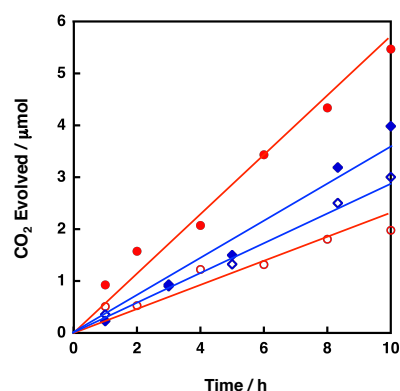


Fig. 8 Time courses of CO₂ evolution under photoirradiation ($\lambda > 340$ nm) of an O₂-saturated aqueous suspension (2.0 mL) containing oxalic acid (10 mM) and metal oxide [11.6 mg; as-prepared K₄Nb₆O₁₇ (red open circle), niobate-NS (red closed circle), as-prepared KTiNbO₅ (blue open diamond) and titanoniobate-NS (blue closed diamond)].

linearly increased with the photoirradiation time for all the catalysts. The CO₂ evolution rate of 0.20 μ mol h⁻¹ for K₄Nb₆O₁₇ was increased to 0.55 μ mol h⁻¹ for niobate-NS by exfoliation. The catalytic activity of niobate-NS was further enhanced by loading QuPh⁺-NA (Fig. S11 in ESI). Similarly, the CO₂ evolution rate for titanoniobate-NS (0.35 μ mol h⁻¹) was larger than that for KTiNbO₅ (0.28 μ mol h⁻¹). Thus, titanoniobate-NS can act as a photocatalyst for oxalic acid oxidation even under acidic conditions.

2.6 Photoinduced electron-transfer state of QuPh⁺-NA (QuPh⁺-NA⁺) on metal oxides detected by EPR spectroscopy.

Photoirradiation of QuPh⁺-NA supported on the metal oxides by a 1000 W high-pressure mercury lamp through a UV-light cutting filter ($\lambda > 340$ nm) results in formation of the triplet ET state (QuPh⁺-NA⁺) via photoinduced electron transfer from the naphthalene (NA) moiety to the singlet excited state of the quinolinium ion (QuPh⁺) moiety as evidenced by EPR measurements at -196 °C. An EPR signal at $g = 2.0031$ appearing under photoirradiation (Fig. 9a) assures formation of a radical species.⁵⁰ The weak EPR signal appeared at $g = 4.0$ assures triplet multiplicity.⁵⁶ The decay rate of the EPR signal of QuPh⁺-NA⁺ observed after cutting off the light highly depends on the metal-oxide supports at room temperature. When redox inactive sAIMCM-41 was used as a support of QuPh⁺-NA, the decay rate in the EPR signal intensity observed after cutting off the light in Fig. 9b (i, black line) is much slower than the decay rate with metal-oxide semiconductors, niobate-NS and titanoniobate-NS (ii, red and iii, blue, respectively). The oscillation of EPR signal intensity during the intermittent photoirradiation for 2 seconds followed by approximately 50 seconds in the dark assures the photorobustness of QuPh⁺-NA on titanoniobate-NS in the presence of water (Fig. 9c).

The shorter lifetime of the ET state of QuPh⁺-NA (QuPh⁺-NA⁺) on the semiconductor nanosheets can be ascribed to facilitated back electron transfer by semiconductor nanosheets, in which QuPh⁺ moiety injected electron to the semiconductor

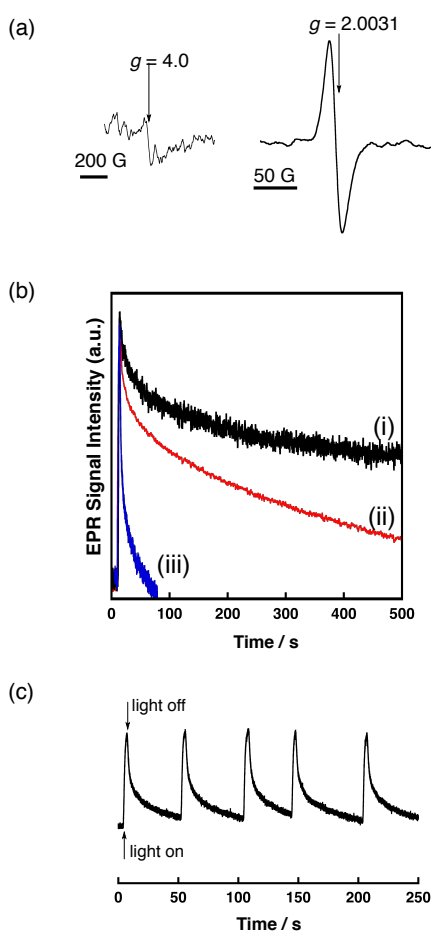


Fig. 9 (a) A typical EPR spectrum of photoinduced $\text{QuPh}^+-\text{NA}^{++}$ on metal oxide ($\text{QuPh}^+-\text{NA}/\text{sAlMCM-41}$) using a high-pressure mercury lamp and cut off filter ($\lambda > 340 \text{ nm}$). (b) Decay time profiles of the EPR signal intensity for $\text{QuPh}^+-\text{NA}^{++}$ supported on (i) mesoporous silica-alumina (black), (ii) niobate-NS (red) and (iii) titanoniobate-NS (blue) at room temperature. (c) Time profiles of the EPR signal intensity for $\text{QuPh}^+-\text{NA}^{++}$ supported on titanoniobate-NS in the presence of water upon intermittent photoirradiation for 2 seconds followed by approximately 50 seconds in the dark at room temperature.

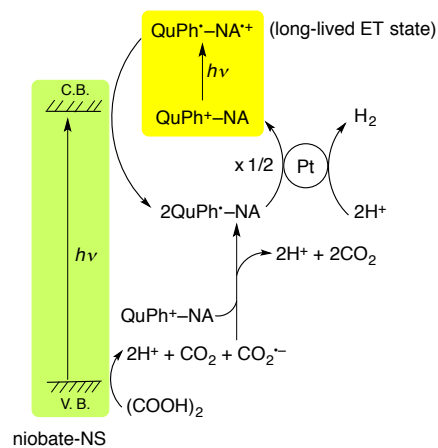
nanosheets and the injected electron reduced NA^{++} moiety. The much faster back electron transfer observed for $\text{QuPh}^+-\text{NA}/\text{titanoniobate-NS}$ compared with that observed for $\text{QuPh}^+-\text{NA}/\text{niobate-NS}$ can be ascribed to the difference in band structures. The band gap of KTiNbO_5 (3.7 eV) which is wider than $\text{K}_4\text{Nb}_6\text{O}_{17}$ (3.5 eV) suggests that the energy of conduction band edge is slightly negative,^{34b} because the valence band of metal-oxide semiconductors typically consists of O 2p orbitals.⁵⁷ The high reducing power of electrons in the conduction band of KTiNbO_5 can accelerate the back electron transfer. Another possible reason for the shorter lifetime of the ET state is the presence of adsorbed water on the surfaces of a metal-oxide semiconductor because the presence of water has been reported to shorten the lifetime of $\text{QuPh}^+-\text{NA}^{++}$ on sAlMCM-41 significantly.⁵⁰ However, TG/DTA analyses of $\text{QuPh}^+-\text{NA}/\text{niobate-NS}$ and $\text{QuPh}^+-\text{NA}/\text{titanoniobate-NS}$ suggest that weight losses due to water desorption were 8.5 and 8.7% for $\text{QuPh}^+-\text{NA}/\text{niobate-NS}$ and $\text{QuPh}^+-\text{NA}/\text{titanoniobate-NS}$, respectively (Fig. S7 in ESI).⁵⁸ The BET surface areas of niobate-NS and titanoniobate-NS are also similar as determined to be $180 \text{ m}^2 \text{ g}^{-1}$ and $166 \text{ m}^2 \text{ g}^{-1}$, respectively. Thus, the effect of adsorbed water on the lifetime of the ET state of QuPh^+-NA on the semiconductors is negligible in this case.

NS, respectively (Fig. S7 in ESI).⁵⁸ The BET surface areas of niobate-NS and titanoniobate-NS are also similar as determined to be $180 \text{ m}^2 \text{ g}^{-1}$ and $166 \text{ m}^2 \text{ g}^{-1}$, respectively. Thus, the effect of adsorbed water on the lifetime of the ET state of QuPh^+-NA on the semiconductors is negligible in this case.

2.7 Reaction mechanisms of photocatalytic H_2 evolution with $\text{QuPh}^+-\text{NA}/\text{KNb}_6\text{O}_{17}\text{-NS}$ (Pt).

The overall photocatalytic cycle of H_2 evolution from oxalic acid with $\text{QuPh}^+-\text{NA}/\text{niobate-NS}$ is depicted in Scheme 1. The photoirradiation of both $\text{K}_4\text{Nb}_6\text{O}_{17}$ and QuPh^+-NA resulted in production of an electron and a hole in the semiconductor and the ET state of QuPh^+-NA , respectively. The long-lived ET state of QuPh^+-NA ($\text{QuPh}^+-\text{NA}^{++}$) was reduced by the electron in the conduction band of niobate-NS and the resulting QuPh^+-NA injects an electron to the Pt catalyst for H_2 evolution. The remaining hole on niobate-NS oxidises oxalic acid by electron transfer. The one-electron oxidised oxalic acid decomposes into CO_2 and CO_2^- together with two protons. The produced CO_2^- reduces QuPh^+-NA to produce QuPh^+-NA .⁴⁸ When photoinactive and insulating sAlMCM-41 was used as a support, no oxidation of acidic oxalic acid occurred with $\text{QuPh}^+-\text{NA}^{++}$, resulting in no photocatalytic H_2 evolution. In the case of titanoniobate-NS used as the support, oxalic acid oxidation proceeded by photoirradiation as shown in Fig. 8. However, the lifetime of the ET state of photogenerated $\text{QuPh}^+-\text{NA}^{++}$ on titanoniobate-NS is dramatically shortened compared with that on niobate-NS (Fig. 9b), resulting in little photocatalytic activity for H_2 evolution (Fig. 7, blue square), because titanoniobate-NS may act as a better electron mediator for back electron transfer from QuPh^+ to NA^{++} than niobate-NS.

Scheme 1 The overall cycle for the photocatalytic H_2 evolution with $\text{QuPh}^+-\text{NA}/\text{niobate-NS}$ (Pt)



3. Conclusions

A composite photocatalyst for H_2 evolution was successfully prepared by rationally arranging an organic electron donor-acceptor dyad (QuPh^+-NA), which forms the long-lived electron transfer state upon photoirradiation, and a Pt catalyst

(proton reduction catalyst) on an appropriate metal-oxide semiconductor nanosheets (niobate-NS), which act as an efficient catalyst for photocatalytic oxidation of oxalic acid. The attractive electrostatic interaction between a Pt catalyst precursor (PtCl_4^{2-}) and QuPh^+-NA on the negatively charged surfaces of niobate-NS resulted in the photoreduction of PtCl_4^{2-} to produce the Pt catalyst, which was closely located to QuPh^+-NA , for efficient H_2 evolution. When semiconductor nanosheets (niobate-NS) were replaced by similar semiconductor nanosheets (titanoniobate-NS), the photocatalytic activity for H_2 evolution was lost because of the much faster back electron transfer in the ET state of QuPh^+-NA via titanoniobate-NS. The composite photocatalyst of an organic electron donor-acceptor dyad and the Pt catalyst supported on semiconductor nanosheets for H_2 evolution developed in this study has paved a new way to combine a wide variety of organic photosynthetic reaction centre models with inorganic photocatalysts for more efficient water splitting that may not be possible by either of photocatalytic component alone.

4. Experimental Section

4.1 Catalyst preparation

4.1.1 Materials. All chemicals were obtained from chemical companies and used without further purification. Potassium tetrachloroplatinate(II) and niobium pentoxide was purchased from Wako Pure Chemical Industries. Tetra(*n*-butyl)ammonium hydroxide were obtained from Tokyo Chemical Industry. Potassium bicarbonate was purchased from Nacalai Tesque. 2-Phenyl-4-(1-naphthyl)quinolinium (QuPh^+-NA) perchlorate was synthesized by a literature method.⁴⁴ Purified water was provided by a Millipore Direct-Q3 ultrapure water system where the electronic conductance was 18.2 M Ω cm. The preparation and characterization of $\text{QuPh}^+-\text{NA}/\text{mesoporous silica-alumina}$ ($\text{QuPh}^+-\text{NA}/\text{sAIMCM-41}$) were reported elsewhere.^{49,50}

4.1.2 Preparation of $\text{K}_4\text{Nb}_6\text{O}_{17}$ nanosheets (niobate-NS). Potassium niobate was prepared by a literature method.^{52,53} Niobium pentoxide (8.6 g, 65 mmol) and potassium bicarbonate (3.1 g, 45 mmol) were ground together in a mortar. The obtained powder was calcined in air at 500 °C for 12 h with a ramp rate of 5 °C min^{-1} . The calcined powder was ground again and calcined at 800 °C and 1000 °C for 12 h each. The obtained powder was washed with water to remove unreacted potassium bicarbonate and dried at 85 °C. The powder X-ray diffraction of the prepared potassium niobate agreed with reported patterns. The as-prepared potassium niobate (4.0 g) was immersed in an aqueous sulphuric acid (4.0 M, 100 mL) and slowly stirred to exchange potassium ions with protons for 1 day. The obtained partially proton-exchanged potassium niobate was immersed and slowly stirred in an aqueous tetra(*n*-butyl)ammonium hydroxide (8.0 wt%, 200 mL) at room temperature for 1 day. Remained precipitate was removed by centrifugation and then the supernatant was acidified with nitric acid to flocculate. The

obtained precipitate was collected by centrifugation, washed with water and dried *in vacuo* overnight.

4.1.3 Preparation of potassium titanoniobate nanosheets (titanoniobate-NS). Potassium titanoniobate was prepared by a literature method.⁵⁵ Titanium dioxide (4.8 g, 60 mmol), niobium pentoxide (8.0 g, 30 mmol) and potassium bicarbonate (4.2 g, 30 mmol) were ground together in a mortar. The obtained powder was calcined at 1000 °C for 12 h with a ramp rate of 5 °C min^{-1} two times. The obtained powder was thoroughly washed with water to remove unreacted potassium bicarbonate and dried at room temperature under reduced pressure. The powder X-ray diffraction of the prepared potassium titanoniobate agreed with reported patterns. The as-prepared potassium titanoniobate (6.0 g) was immersed in an aqueous hydrosulphuric acid (4.0 M, 100 mL) and slowly stirred for 1 day. The obtained partially proton exchanged potassium titanoniobate was immersed and slowly stirred in an aqueous tetra(*n*-butyl)ammonium hydroxide (10 wt%, 200 mL) at room temperature for 1 day. Remained precipitate was removed by centrifugation and then, the supernatant was acidified with nitric acid to flocculate. The obtained precipitates were collected by centrifugation, washed with water and dried *in vacuo* overnight.

4.1.4 Preparation of $\text{QuPh}^+-\text{NA}/\text{niobate-NS}$ and $\text{QuPh}^+-\text{NA}/\text{titanoniobate-NS}$. QuPh^+-NA ion was supported on niobate-NS or titanoniobate-NS by a cation-exchange method in a mixed solution of acetonitrile and water.^{49,50,56} niobate-NS or titanoniobate-NS (100 mg) was dispersed to a mixed solution of acetonitrile and water [1:1 (v/v)] containing QuPh^+-NA (3.0 mM). The amount of exchanged QuPh^+-NA ion was calculated based on the decrease in absorbance at 334 nm characteristic to QuPh^+-NA ion caused by immersion of niobate-NS or titanoniobate-NS.

4.2 Catalyst characterization

4.2.1 Transmission Electron Microscopy (TEM). Metal-oxide semiconductors were observed from bright field images using a JEOL JEM-2100 that has a thermal field emission gun with an accelerating voltage of 200 kV. The observed samples were prepared by dropping an aqueous suspension of metal-oxide semiconductors and allowing the solvent to evaporate and then scooped up with an amorphous carbon supporting film on a meshed Cu grid.

4.2.2 Electron paramagnetic resonance (EPR). The EPR spectra were taken on a JEOL X-band spectrometer (JES-REIXE) with a quartz EPR tube (4.5 mm). The EPR spectrum of the ET state of QuPh^+-NA supported on a metal oxide support, which were dried under vacuum overnight, was measured under photoirradiation with high-pressure mercury lamp (USH-1005D) through both a UV-light ($\lambda < 340$ nm) cut glass filter and a water filter (light path length: 3 cm) to cut off the IR irradiation for focusing at the sample cell in the EPR cavity at room temperature. The *g* values were calibrated using an Mn^{2+} marker.

4.2.3 XRD, TG/DTA and DRS. Powder X-ray diffraction patterns were recorded on a Rigaku MiniFlex 600. Incident X-ray radiation was produced by a Cu X-ray tube, operating at 40

kV and 15 mA with Cu $K\alpha$ radiation ($\lambda = 1.54 \text{ \AA}$). The scan rate was 2° min^{-1} from $2\theta = 10\text{--}50^\circ$. TG/DTA measurements were performed on a SII TG/DTA 7200. A sample (about 10 mg) was loaded into an Al pan and heated under air with continuous flowing. A certain amount of $\gamma\text{-Al}_2\text{O}_3$ was used as a reference for DTA measurements. The sample temperature was increased with the rate of $2.5^\circ \text{ C min}^{-1}$. Nitrogen-adsorption/desorption measurements were performed at -196° C on a Belsorp-mini (BEL Japan, Inc.) within the relative pressure range 0.01–101.3 kPa. A sample mass of about 30 mg was used for the adsorption analysis after pretreatment at 150° C for several hours under vacuum conditions and kept under a N_2 atmosphere for the N_2 -adsorption measurements. The sample was exposed to a mixed He/N_2 gas flow with a programmed ratio and the amount of adsorbed N_2 was calculated from the change of pressure in a cell after reaching equilibrium. Diffuse reflectance UV-vis absorption spectra were recorded by a Jasco V-670 spectrometer equipped with an SIN-768 attachment. BaSO_4 was used for recording background spectra.

4.3 Photocatalytic H_2 evolution

A typical experimental procedure is as follows: an aqueous suspension (2.0 mL) containing $\text{QuPh}^+\text{-NA}/\text{niobate-NS}$ composite (10.5 mg, $\text{QuPh}^+\text{-NA}$: 0.74 mM), K_2PtCl_4 (10 μM) and oxalic acid (50 mM) was flushed with N_2 gas. The suspension was then photoirradiated for a certain time with a xenon lamp (Ushio Optical, Model X SX-UID 500X AMQ) through a colour filter glass (Asahi Techno Glass L39) transmitting $\lambda > 340 \text{ nm}$ at room temperature. After 1 min stirring in the dark, gas in a headspace was analysed by Shimadzu GC-14B gas chromatography (detector: TCD, column temperature: 50° C , column: active carbon with the particle size 60-80 mesh, carrier gas: N_2 gas) to determine the amount of evolved H_2 .

Acknowledgements

This work was supported by Grants-in-Aid (Nos. 24350069 and 25600025) for Scientific Research from Japan Society for the Promotion of Science (JSPS), an ALCA project from Japan Science and Technology Agency (JST), and NRF of Korea through the GRL (2010-00353) program. We sincerely acknowledge the Research Centre for Ultra-Precision Science & Technology, Osaka University for TEM measurements.

Notes and references

Department of Material and Life Science, Graduate School of Engineering, Osaka University, ALCA, Japan Science and Technology Agency (JST), Suita, Osaka 565-0871, Japan

E-mail: fukuzumi@chem.eng.osaka-u.ac.jp

Electronic Supplementary Information (ESI) available: N_2 adsorption-desorption isotherm (Figs. S1 and S6), powder X-ray diffraction (Figs. S2 and S3), time course of DRS absorbance change (Fig. S4), TG/DTA curves (Figs. S5 and S7), IR spectra (Fig. S8), TEM images (Fig. 9), time course of H_2 evolution (Fig. S10) and time course of CO_2 evolution in oxalate oxidation (Fig. S11). See DOI: 10.1039/b000000x/

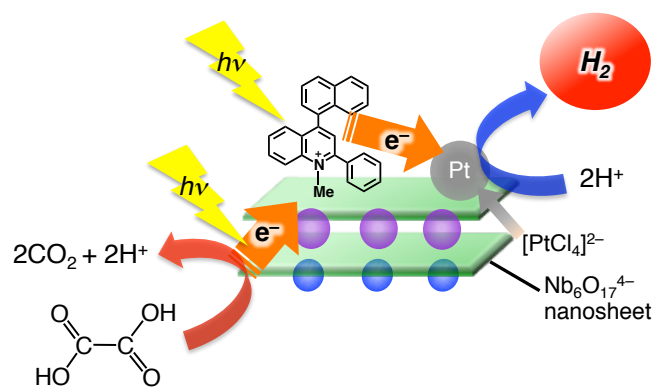
- (a) S. Dunn, in *Encyclopedia of Energy*, Elsevier Inc., 2004, vol. 3, pp. 241-252; (b) M. Momirlan and T. N. Veziroglu, *Int. J. Hydrogen Energy*, 2005, **30**, 795-802; (c) *The Hydrogen Economy: Opportunities, Costs, Barriers, and R&D Needs*, 2004, U.S. National Research Council and U.S. National Academy of Engineering.
- G. Laurenczy, in *Encyclopedia of Catalysis*, ed. I. T. Horvath, Wiley-Interscience, Hoboken, NJ, 2010.
- (a) H. B. Gray, *Nat. Chem.*, 2009, **1**, 7-7; (b) N. S. Lewis and D. G. Nocera, *Proc. Natl. Acad. Sci. U. S. A.*, 2006, **103**, 15729-15735; (c) D. G. Nocera, *Chem. Soc. Rev.*, 2009, **38**, 13-15; (d) T. A. Faunce, W. Lubitz, A. W. B. Rutherford, D. MacFarlane, G. F. Moore, P. Yang, D. G. Nocera, T. A. Moore, D. H. Gregory, S. Fukuzumi, K. B. Yoon, F. A. Armstrong, M. R. Wasielewski and S. Styring, *Energy Environ. Sci.*, 2013, **6**, 695-698
- (a) Y. Amao, *ChemCatChem*, 2011, **3**, 458-474; (b) P. D. Tran, L. H. Wong, J. Barber and J. S. C. Loo, *Energy Environ. Sci.*, 2012, **5**, 5902-5918; (c) S. Bensaid, G. Centi, E. Garrone, S. Perathoner and G. Saracco, *ChemSusChem*, 2012, **5**, 500-521.
- (a) D. G. Nocera, *Acc. Chem. Res.*, 2012, **45**, 767-776; (b) M. Wang, L. Chen and L. Sun, *Energy Environ. Sci.*, 2012, **5**, 6763-6778; (c) S. Y. Reece, J. A. Hamel, K. Sung, T. D. Jarvi, A. J. Esswein, J. J. H. Pijpers and D. G. Nocera, *Science*, 2011, **334**, 645-648.
- (a) R. M. Bullock, A. M. Appel and M. L. Helm, *Chem. Commun.*, 2014, **50**, 3125-3143; (b) P. V. Kamat, *J. Phys. Chem. C*, 2007, **111**, 2834-2860; (c) A. J. Bard and M. A. Fox, *Acc. Chem. Res.*, 1995, **28**, 141-145; (d) Y. Qu and X. Du, *Chem. Soc. Rev.*, 2013, **42**, 2568-2580.
- (a) Y. Halpin, M. T. Pryce, S. Rau, D. Dinic and J. G. Vos, *Dalton Trans.*, 2013, **42**, 16243-16254; (b) P. D. Frischmann, K. Mahata and F. Wüthner, *Chem. Soc. Rev.*, 2013, **42**, 1847-1870. (c) B. van den Bosch, H.-C. Chen, J. I. van der Vlugt, A. M. Brouwer and J. N. H. Reek, *ChemSusChem*, 2013, **6**, 790-793.
- (a) S. Fukuzumi, *Eur. J. Inorg. Chem.*, 2008, 1351-1362; (b) V. S. Thoi, Y. Sun, J. R. Long and C. J. Chang, *Chem. Soc. Rev.* 2013, **42**, 2388-2400; (c) S. Fukuzumi, Y. Yamada, T. Suenobu, K. Ohkubo and H. Kotani, *Energy Environ. Sci.*, 2011, **4**, 2754-2766.
- (a) A. Fujishima and K. Honda, *Nature*, 1972, **238**, 37; (b) A. Fujishima, X. Zhang and D. A. Tryk, *Int. J. Hydrogen Energy*, 2007, **32**, 2664.
- (a) A. Kudo and Y. Miseki, *Chem. Soc. Rev.*, 2009, **38**, 253-278; (b) A. Kudo, *Int. J. Hydrogen Energy*, 2007, **32**, 2673.
- (a) K. Takanabe and K. Domen, *ChemCatChem*, 2012, **4**, 1485-1497; (b) K. Maeda and K. Domen, *J. Phys. Chem. Lett.*, 2010, **1**, 2655-2661.
- F. E. Osterloh, *Chem. Mater.*, 2008, **20**, 35-54.
- X. Chen, S. Shen, L. Guo and S. S. Mao, *Chem. Rev.*, 2010, **110**, 6503-6570.
- J. S. Lee, *Catal. Surv. Asia*, 2006, **9**, 217-227.
- M. G. Walter, E. L. Warren, J. R. McKone, S. W. Boettcher, Q. Mi, E. A. Santori and N. S. Lewis, *Chem. Rev.*, 2010, **110**, 6446-6473.
- H. Zhou, T. Fan and D. Zhang, *ChemSusChem*, 2011, **3**, 513-528.
- J. Yang, D. Wang, H. Han, A. C. Li, *Acc. Chem. Res.*, 2013, **46**, 1900-1909.
- P. F. Ji, M. Takeuchi, T. M. Cuong, J. L. Zhang, M. Matsuoka and M. Anpo, *Res. Chem. Intermed.*, 2010, **36**, 327-347.

- 19 R. M. Navarro, M. C. Alvarez-Galvan, J. A. V. de la Mano, S. M. Al-Zahrani and J. L. G. Fierro, *Energy Environ. Sci.*, 2010, **3**, 1865-1882.
- 20 R. M. N. Yerga, M. C. A. Galvan, F. del Valle, J. A. V. de la Mano and J. L. Fierro, *ChemSusChem*, 2009, **2**, 471-485.
- 21 H. Kato, K. Asakura and A. Kudo, *J. Am. Chem. Soc.*, 2003, **125**, 3082-3089.
- 22 (a) K. Domen, A. Kudo, A. Shinozaki, A. Tanaka, K. Maruya and T. Onishi, *J. Chem. Soc., Chem. Commun.*, 1986, 356; (b) K. Domen, A. Kudo, M. Shibata, A. Tanaka, K. Maruya and T. Onishi, *J. Chem. Soc., Chem. Commun.*, 1986, 1706-1707.
- 23 (a) A. Kudo, A. Tanaka, K. Domen, K. Maruya, K. Aika and T. Onishi, *J. Catal.*, 1988, **111**, 67-76; (b) A. Kudo, K. Sayama, A. Tanaka, K. Asakura, K. Domen, K. Maruya and T. Onishi, *J. Catal.*, 1989, **120**, 337-352.
- 24 (a) K. Sayama, A. Tanaka, K. Domen, K. Maruya and T. Onishi, *Catal. Lett.*, 1990, **4**, 217-222; (b) K. Sayama, A. Tanaka, K. Domen, K. Maruya and T. Onishi, *J. Phys. Chem.*, 1991, **95**, 1345-1348; (c) K. Sayama, K. Yase, H. Arakawa, K. Asakura, A. Tanaka, K. Domen and T. Onishi, *J. Photochem. Photobiol. A*, 1998, **114**, 125-135.
- 25 (a) J. Hou, Z. Wang, W. Kan, S. Jiao, H. Zhu and R. V. Kumar, *J. Mater. Chem.*, 2012, **22**, 7291-7299; (b) J. E. Yourey, J. B. Kurtz and B. M. Bartlett, *J. Phys. Chem. C*, 2012, **116**, 3200-3206; (c) P. Lei, F. Wang, S. Zhang, Y. Ding, J. Zhao and M. Yang, *ACS Appl. Mater. Interfaces*, 2014, **6**, 2370-2376.
- 26 (a) Y. Moriya, T. Takata and K. Domen, *Coord. Chem. Rev.*, 2013, **257**, 1957-1969; (b) K. Maeda, D. Lu and K. Domen, *Chem.-Eur. J.*, 2013, **19**, 4986-4991; (c) M. Higashi, K. Domen and R. Abe, *J. Am. Chem. Soc.* 2012, **134**, 6968-6971; (d) K. Maeda and K. Domen, *J. Phys. Chem. C*, 2007, **111**, 7851-7861; (e) K. Maeda, K. Teramura and K. Domen, *J. Catal.*, 2008, **254**, 198-204.
- 27 A. J. Bard, *J. Photochem.*, 1979, **10**, 59-75.
- 28 (a) R. Abe, K. Shinmei, N. Koumura, K. Hara and B. Ohtani, *J. Am. Chem. Soc.*, 2013, **135**, 16872-16884; (b) R. Abe, K. Sayama, K. Domen and H. Arakawa, *Chem. Phys. Lett.*, 2001, **344**, 339-344; (c) R. Abe, *J. Photochem. Photobiol. C*, 2011, **11**, 179-209.
- 29 W. Fan, Q. Zhang and Y. Wang, *Phys. Chem. Chem. Phys.*, 2013, **15**, 2632-2649.
- 30 K. Sayama, K. Mukasa, R. Abe, Y. Abe and H. Arakawa, *Chem. Commun.*, 2001, 2416-2417.
- 31 (a) A. Kudo, *MRS Bull.*, 2011, **36**, 32-38; (b) Q. Jia, A. Iwase and A. Kudo, *Chem. Sci.*, 2014, **5**, 1513-1519; (c) Y. Sasaki, A. Iwase, H. Kato and A. Kudo, *J. Catal.*, 2008, **259**, 133-137; (d) Y. Sasaki, H. Kato and A. Kudo, *J. Am. Chem. Soc.*, 2013, **135**, 5441-5449.
- 32 (a) K. Maeda, M. Higashi, D. Lu, R. Abe and K. Domen, *J. Am. Chem. Soc.*, 2010, **132**, 5858-5868; (b) K. Maeda, R. Abe and K. Domen, *J. Phys. Chem. C*, 2011, **115**, 3057-3064; (c) K. Maeda, *ACS Catal.*, 2013, **3**, 1486-1503.
- 33 H. Gerischer, *J. Photochem. Photobiol.*, 1972, **16**, 243-260.
- 34 (a) Y. I. Kim, S. Salim, M. J. Huq and T. E. Mallouk, *J. Am. Chem. Soc.*, 1991, **113**, 9561-9563; (b) Y. I. Kim, S. J. Atherton, E. S. Brigham and T. E. Mallouk, *J. Phys. Chem.*, 1993, **97**, 11802-22810; (c) W. J. Youngblood, S.-H. A. Lee, K. Maeda and T. E. Mallouk, *Acc. Chem. Res.*, 2009, **42**, 1966-1973.
- 35 T. Nakato, K. Kuroda and C. Kato, *Chem. Mater.*, 1992, **4**, 128-132.
- 36 K. Mori, S. Ogawa, M. Martis and H. Yamashita, *J. Phys. Chem. C*, 2012, **116**, 18873-18877.
- 37 T. K. Townsend, E. M. Sabio, N. D. Browning and F. E. Osterloh, *ChemSusChem*, 2011, **4**, 185-190.
- 38 S. Uchida, Y. Yamamoto, Y. Fujishiro, A. Watanabe, O. Ito and T. Sato, *J. Chem. Soc., Faraday Trans.*, 1997, **93**, 3229-3234.
- 39 K. Maeda, M. Eguchi, W. J. Youngblood and T. E. Mallouk, *Chem. Mater.*, 2008, **20**, 6770-6778.
- 40 (a) H. Hagiwara, T. Inoue, K. Kaneko and T. Ishihara, *Chem.-Eur. J.*, 2009, **15**, 12862-12870; (b) H. Hagiwara, M. Nagatomo, C. Seto, S. Ida and T. Ishihara, *J. Photochem. Photobiol. A*, 2013, **272**, 41-48; (c) H. Hagiwara, T. Inoue, S. Ida and T. Ishihara, *Phys. Chem. Chem. Phys.*, 2011, **13**, 18031-18037.
- 41 (a) M. R. Wasielewski, *Acc. Chem. Res.*, 2009, **42**, 1910-1921; (b) D. Gust, T. A. Moore and A. L. Moore, *Acc. Chem. Res.*, 2009, **42**, 1890-1898; (c) D. Gust, T. A. Moore and A. L. Moore, *Acc. Chem. Res.*, 1993, **26**, 198-205.
- 42 (a) S. Fukuzumi, K. Ohkubo and T. Suenobu, *Acc. Chem. Res.*, 2014, **47**, 1455-1464; (b) S. Fukuzumi, *Phys. Chem. Chem. Phys.*, 2008, **10**, 2283-2297; (c) S. Fukuzumi and K. Ohkubo, *J. Mater. Chem.*, 2012, **22**, 4575-4587; (d) S. Fukuzumi, *Org. Biomol. Chem.*, 2003, **1**, 609-620.
- 43 S. Fukuzumi, H. Kotani, K. Ohkubo, S. Ogo, N. V. Tkachenko and H. Lemmetyinen, *J. Am. Chem. Soc.*, 2004, **126**, 1600-1601.
- 44 H. Kotani, K. Ohkubo and S. Fukuzumi, *Faraday Discuss.*, 2012, **155**, 89-102.
- 45 (a) H. Kotani, K. Ohkubo, Y. Takai and S. Fukuzumi, *J. Phys. Chem. B*, 2006, **110**, 24047-24053; (b) H. Kotani, T. Ono, K. Ohkubo and S. Fukuzumi, *Phys. Chem. Chem. Phys.*, 2007, **9**, 1487-1492; (c) H. Kotani, R. Hanazaki, K. Ohkubo, Y. Yamada and S. Fukuzumi, *Chem.-Eur. J.*, 2011, **17**, 2777-2785.
- 46 (a) Y. Yamada, T. Miyahigashi, H. Kotani, K. Ohkubo and S. Fukuzumi, *J. Am. Chem. Soc.*, 2011, **133**, 16136-16145; (b) Y. Yamada, S. Shikano and S. Fukuzumi, *J. Phys. Chem. C*, 2013, **117**, 13143-13152.
- 47 Y. Yamada, T. Miyahigashi, H. Kotani, K. Ohkubo and S. Fukuzumi, *Energy Environ. Sci.*, 2012, **5**, 6111-6118.
- 48 Y. Yamada, T. Miyahigashi, K. Ohkubo and S. Fukuzumi, *Phys. Chem. Chem. Phys.*, 2012, **14**, 10564-10571.
- 49 Y. Yamada, H. Tadokoro and S. Fukuzumi, *RSC Adv.*, 2013, **3**, 25677-25680.
- 50 Y. Yamada, A. Nomura, K. Ohkubo, T. Suenobu and S. Fukuzumi, *Chem. Commun.*, 2013, **49**, 5132-5134.
- 51 (a) D. B. Haytowitz and R. H. Matthews, *Agriculture Handbook No. 8-11*, Science and Education Administration, USDA, Washington, D.C., 1984; (b) E. A. Malinka and G. L. Kamalov, *React. Kinet. Catal. Lett.*, 1993, **52**, 13-18; (c) E. A. Malinka and G. L. Kamalov, *J. Photochem. Photobiol. A: Chem.*, 1994, **81**, 193-197; (d) E. A. Malinka, G. L. Kamalov, S. V. Vodzinskii, V. I. Melnik and Z. I. Zhilina, *J. Photochem. Photobiol. A: Chem.*, 1995, **90**, 153-158.
- 52 K. Nassau, J. W. Shiever and J. L. Bernstein, *J. Electrochem. Soc.*, 1969, **116**, 348-353.
- 53 A. D. Wadsley, *Acta Cryst.*, 1964, **17**, 623-628.
- 54 G. H. Du, Y. Yu, Q. Chen, R. H. Wang, W. Zhou and L. M. Peng, *Chem. Phys. Lett.*, 2003, **377**, 445-448.
- 55 R. C. Weast, In *Handbook of Chemistry and Physics, 56 Ed.*, CRC, Cleveland, OH, 1975-1976.

ARTICLE

- 56 S. Fukuzumi, K. Doi, A. Itoh, T. Suenobu, K. Ohkubo, Y. Yamada and K. D. Karlin, *Proc. Natl. Acad. Sci. U. S. A.*, 2012, **109**, 15572-15577.
- 57 D. E. Scaife, *Solar Energy*, 1980, **25**, 41-54.
- 58 M. A. Bizeto and V. R. L. Constantino, *Mater. Res. Bull.*, 2004, **39**, 1729-1736.

Table of Contents



A Pt catalyst was closely located to an organic photosensitizer on a negatively charged semiconductor for efficient photocatalytic H_2 evolution.